Published in final edited form as:
Proc IEEE Ultrason Symp. 2010 October 11; 2010: 375–377. doi:10.1109/ULTSYM.2010.5935647.

3-D Deep Penetration Photoacoustic Imaging with a 2-D CMUT Array

Te-Jen Ma[1], **Sri Rajasekhar Kothapalli**[2], **Srikant Vaithilingam**[1], **Ömer Oralkan**[1], **Aya Kamaya**[3], **Ira O. Wygant**[1], **Xuefeng Zhuang**[1], **Sanjiv S. Gambhir**[2], **R. Brooke Jeffrey Jr.**[3], and **Butrus T. Khuri-Yakub**[1]

[1] Edward L. Ginzton Laboratory, Stanford University, USA

[2] Department of Radiology, Molecular Imaging Program, Stanford University, USA

[3] Department of Radiology, Stanford University Medical Center, Stanford University, USA

Abstract

In this work, we demonstrate 3-D photoacoustic imaging of optically absorbing targets embedded as deep as 5 cm inside a highly scattering background medium using a 2-D capacitive micromachined ultrasonic transducer (CMUT) array with a center frequency of 5.5 MHz. 3-D volumetric images and 2-D maximum intensity projection images are presented to show the objects imaged at different depths. Due to the close proximity of the CMUT to the integrated frontend circuits, the CMUT array imaging system has a low noise floor. This makes the CMUT a promising technology for deep tissue photoacoustic imaging.

I. Introduction

Photoacoustic imaging (PAI) is a medical imaging modality that has drawn increasing attention in the past decade [1]. In PAI, nanosecond pulsed light propagating through biological tissue is absorbed by chromophores such as oxy and de-oxy hemoglobin. This absorption and the subsequent thermo-elastic expansion creates broadband ultrasonic waves, which are then captured with an acoustic transducer. Photoacoustic images provide speckle free and rich optical contrast images at ultrasonic resolution. PAI can also provide functional information such as the ability to differentiate between arteries and veins by using the differential absorption of oxy and deoxyhemoglobin [2]. These images can be further enhanced with the use of exogenous contrast agents such as carbon nanotubes which can be targeted to attach to specific molecules of interest [3]. One of the main challenges of photoacoustic imaging has been limited depth penetration. Deep tissue imaging is very important for applications such as breast and prostate cancer diagnosis, for which a penetration depth around 5 cm is desired. Because of the miniature size and integrated front-end electronics, CMUTs are ideal fit for endoscopic applications. We have previously demonstrated that capacitive micromachined ultrasonic transducers (CMUTs) are capable of performing PAI [4] [5]. This paper investigates the deep tissue photoacoustic imaging capability of CMUTs.

II. Methods

A. 2-D CMUT Array and Integrated Electronics

A 2-D CMUT array flip-chip bonded to a custom-designed ASIC is utilized. The 2-D CMUT array was fabricated with sacrificial layer etch process [6]. The ASIC provides the circuitry for transmitting and pre-amps for receiving. Details of the ASIC design can be found in [7]. Having the IC flip-chip bonded directly to the CMUT is important since it

greatly alleviates the parasitic cable capacitance and the noise generated when using a longer electrical transmission path [7]. Pulse-echo characterization from an oil-air interface showed that this CMUT has a center frequency of 5.5 MHz and a fractional bandwidth of 101% (Fig. 1).

B. Experimental Setup

The imaging experiments were carried out in a setup as shown in Fig. 2. First, a laser beam with about 2 cm diameter was used to irradiate an imaging object holder by a free space optical setup. The laser source was a tunable optical parametric oscillator (OPO) pumped by a Q-switched Nd:YAG laser (Continuum SLIII-10). The laser pulses have a width of 6 ns and a repetition rate of 10 Hz. For this particular experiment, the laser wavelength was 750 nm and the laser power was 14.1 mJ/cm^2, which is below the ANSI safety limit for human skin exposure.

Then, the imaging object holder was suspended stationary inside an oil tank to ensure proper ultrasound coupling. Oil was used because it is non-conductive and can insulate the exposed electronic circuits. The phantom holder was made of acrylic pieces with 0.25 inch thickness. The 16 × 16 CMUT array that is fixed to the oil tank and is below the imaging phantom was manually scanned in x and y directions 4 times respectively to simulate the aperture of a 64 × 64 CMUT array. This system was aligned carefully before the experiment to minimize the phase distortion due to the manual scanning.

For the experiment, 4 absorbing targets were embedded inside a gel of 1% Intralipid (20% Liposyn II) background medium mixed with 1% agar. The background medium has a reduced scattering coefficient of around 10/cm, which closely resembles that of biological tissue. Each absorbing target consists 3 strands of 150 μm thick horse hair to create an arrow shaped object. The arrow-shaped strands of horse hair were embedded inside the gel at four different depths, from 3.5 cm deep to 5 cm deep with 0.5-cm depth spacing. As shown in Fig. 2, these objects were placed diagonally inside the medium, so that the light and ultrasound propagate about the same distance inside the medium, although along different paths. This partially simulates a reflection geometry imaging setup where the light and the sound also travel the same distance inside the medium. In a reflection geometry setup, however, the light source and ultrasound detector are on the same side with respect to the phantom/subject.

During scanning, A-scan signals were captured with an 8-bit digitizer card (National Instrument PCI-5114) and averaged 4 times at each data point. The A-scans were stored on a computer for offline processing.

C. Image Reconstruction

Images of the phantom were reconstructed using the synthetic aperture focusing technique. First, the A-scan signals were band-pass filtered before being appropriately delayed and summed. The beamformed image was then multiplied by a coherence factor weighting [8], [9]. A coherence factor weighting is used to reduce the focusing error due to the sound velocity inhomogeneities. Finally, the signals were log compressed to the appropriate dynamic range for display purposes.

III. Results and Discussion

As shown in Fig. 4, the horse hairs were oriented in different directions at different depths inside the phantom. Figs. 5(a) and 5(b) show the 3-D reconstructed volumetric image of the phantom. These results show that the horse hairs at the four different depths (3.5 cm, 4 cm, 4.5 cm and 5 cm) inside the phantom can be easily resolved. The orientation of these hairs in

the image is in accordance with phantom photographs shown in Fig. 4. 3-D volumetric images and 2-D cross-sectional slices are shown using medical image viewing software (Volview 3.2, Kitware). In Figs 5(c) and 5(d), we show line plots (as a function of depth) of the horse hairs embedded at the depths of 3.5 cm and 5 cm respectively. These line plots are represented in dB. Table 1 shows spatial resolution (axial and lateral) as a function of imaging depth. For 5-cm object, SNR and spatial resolution are approximately 40 dB and 700 μm respectively. We could not achieve uniform illumination over the entire scanning range, as the laser beam is fixed in our experimental setup (centered around a depth of 4cm in the phantom). This can be improved in a future experimental setup if the light ring is built around the CMUT array so that both light and CMUT are scanned together

IV. Conclusion

This work demonstrated the capability of a 2-D CMUT array to perform photoacoustic imaging of light absorbing objects embedded as deep as 5 cm inside a tissue-mimicking phantom. The laser energy applied was 70% of the ANSI limit. Our results show that the CMUT is capable of performing deep tissue imaging. This high depth sensitivity is aided by the fact that the CMUT has an ASIC flip-chip bonded to the transducer array directly. The close proximity of the front-end electronics to the CMUT mitigates the parasitics and improves the noise performance. These results make the CMUT a promising candidate for photoacoustic imaging applications such as prostate cancer or colon cancer imaging.

Acknowledgments

This work was performed using funds by Canon Inc. and National Institute of Health. National Semiconductor provided the fabrication of the integrated circuits. Dr. Kothapalli is supported by Hamalainen Pelican Postdoctoral Fellowship from Sir Peter and Lady Michael Foundation. Srikant Vaithilingam was supported by a P. Michael Farmwald Stanford Graduate Fellowship. Dr. Xuefeng Zhuang was supported by a Weiland Family Stanford Graduate Fellowship. CMUT fabrication was done at the Stanford Nanofabrication Facility (Stanford, CA), which is a member of National Nanotechnology Infrastructure Network.

References

1. Wang X, Pang Y, Ku G, Xie X, Stoica G, Wang LV. Non-invasive laser-induced photoacoustic tomography for structural and functional imaging of the brain in vivo. Nature Biotechnology. Jul; 2003 21(7):803–806.
2. Zhang HF, Maslov K, Stoica G, Wang LV. Functional photoacoustic microscopy for high-resolution and noninvasive in vivo imaging. Nature Biotechnology. Jul.2006 24:848–851.
3. de la Zerda A, Zavaleta C, Keren S, Vaithilingam S, Bodapati S, Liu Z, Levi J, Smith BR, Ma TJ, Oralkan O, Cheng Z, Chen X, Dai H, Khuri-Yakub BT, Gambhir SS. Carbon nanotubes as photoacoustic molecular imaging agents in living mice. Nature Nanotechnology. Sep.2008 3:557–562.
4. Wygant, IO.; Zhuang, X.; Kuo, PS.; Yeh, DT.; Oralkan, O.; Khuri-Yakub, BT. Photoacoustic imaging using a two-dimensional CMUT array. Proc IEEE Ultrason Symp; Rotterdam, Netherlands. Sept. 2005 p. 1921-1924.
5. Vaithilingam S, Ma T-J, Furukawa Y, Wygant IO, Zhuang X, de la Zerda A, Oralkan Ö, Kamaya A, Gambhir SS, Jeffrey RB Jr, Khuri-Yakub BT. Three-dimensional photoacoustic imaging using a two-dimensional CMUT array. Ultrasonics, Ferroelectrics and Frequency Control, IEEE Transactions. Nov; 2009 56(11):2411–19.
6. Ergun AS, Huang Y, Zhuang X, Oralkan O, Yarahoglu GG, Khuri-Yakub BT. Capacitive micromachined ultrasonic transducers: fabrication technology. Ultrasonics, Ferroelectrics and Frequency Control, IEEE Transactions. Dec; 2005 52(12):2242–2258.
7. Wygant I, Zhuang X, Yeh D, Oralkan Ö, Ergun AS, Karaman M, Khuri-Yakub BT. Integration of 2D CMUT arrays with front-end electronics for volumetric ultrasound imaging. Ultrasonics, Ferroelectrics and Frequency Control, IEEE Transactions. Feb; 2008 55(2):327–342.

8. Li PC, Li ML. Adaptive imaging using the generalized coherence factor. Ultrasonics, Ferroelectrics and Frequency Control, IEEE Transactions. Feb; 2003 50(2):128–141.

9. Liao CK, Li ML, Li PC. Optoacoustic imaging with synthetic aperture focusing and coherence weighting. Opt Lett. 2004; 29(21):2506–2508. [PubMed: 15584276]

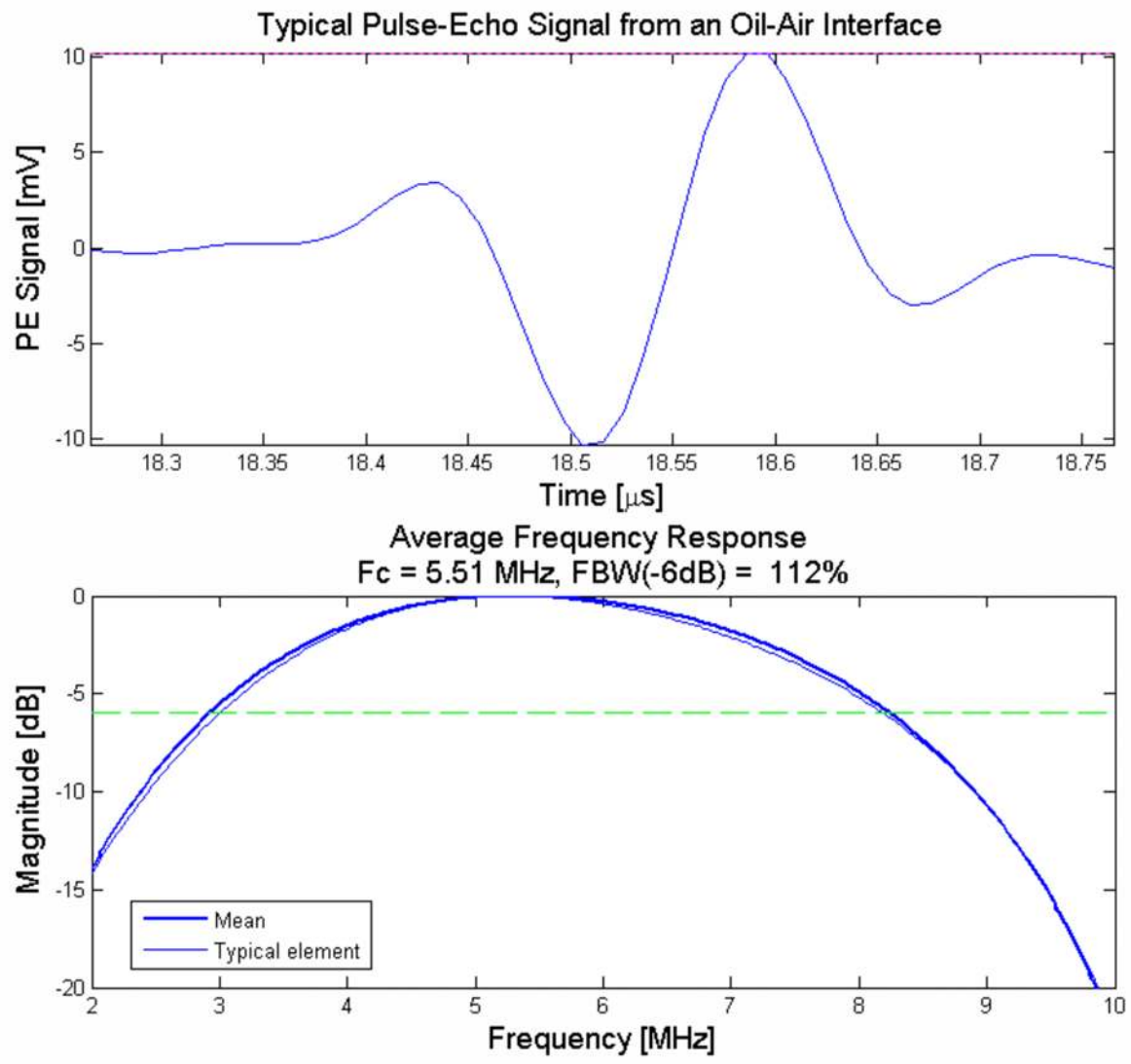

Fig. 1.
Impulse response from one of the typical CMUT elements on the 2-D CMUT array.

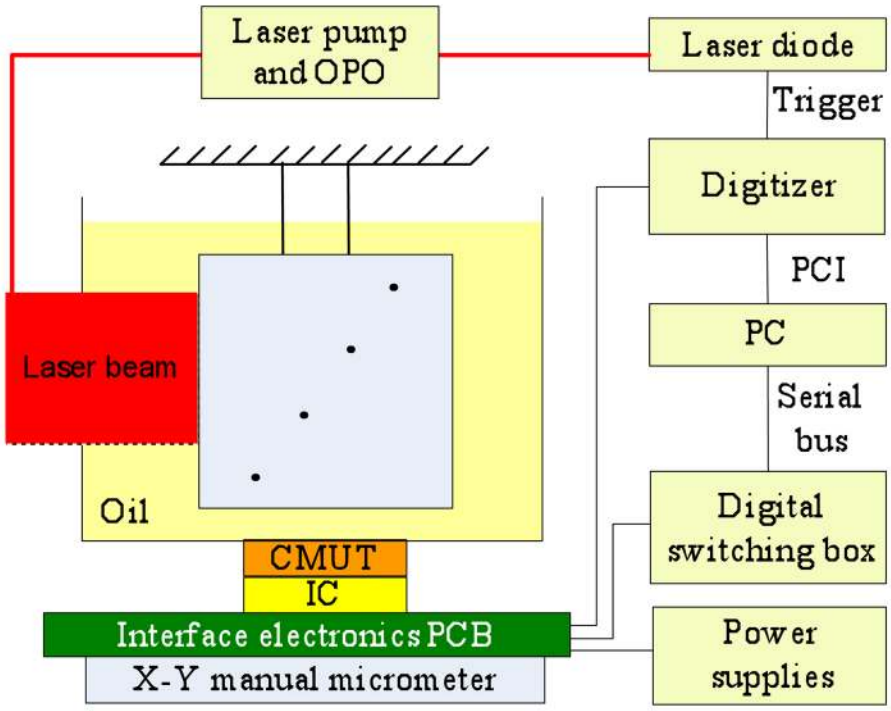

Fig. 2.

The experimental setup. Laser beam was delivered with a free space setup. The wavelength was at 750 nm and the power was 14.1 mJ/cm^2. The CMUT was fixed on top of an X–Y micrometer, which enables manual scanning. The phantom holder was suspended stationary inside an oil tank with horse hair pieces embedded inside the 1% Intralipid solution.

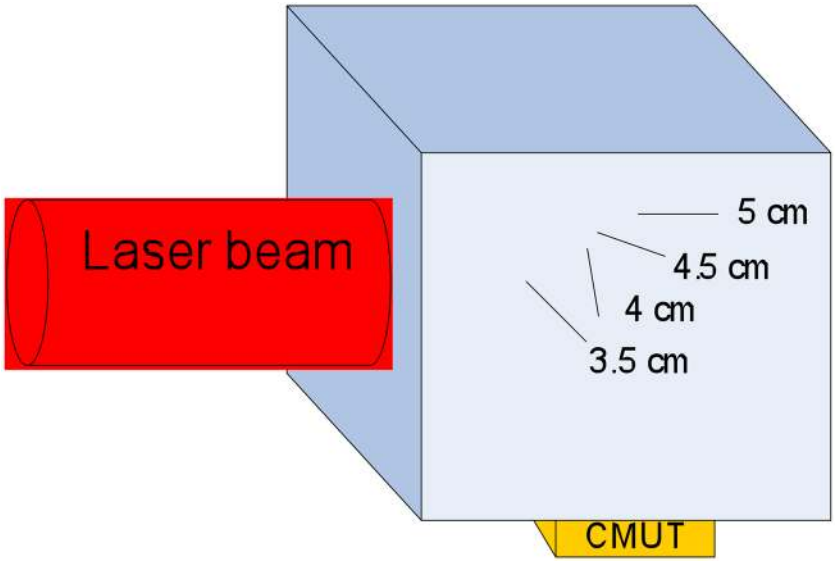

Fig. 3.
Schmatic of light and ultrasound positions with respect to the horse hair strands placed at 3.5 cm, 4 cm, 4.5 cm, and 5 cm deep inside the phantom. The distance is the same for optical penetration and acoustical penetration.

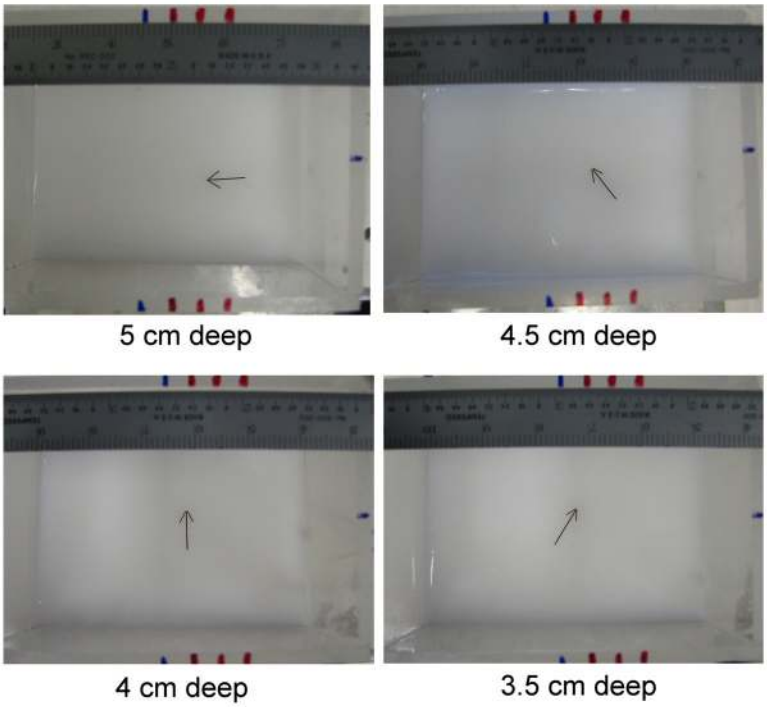

Fig. 4.
Optical pictures of the horse hair strands with a diameter of 150 μm placed at 3.5 cm, 4 cm, 4.5 cm and 5 cm depth.

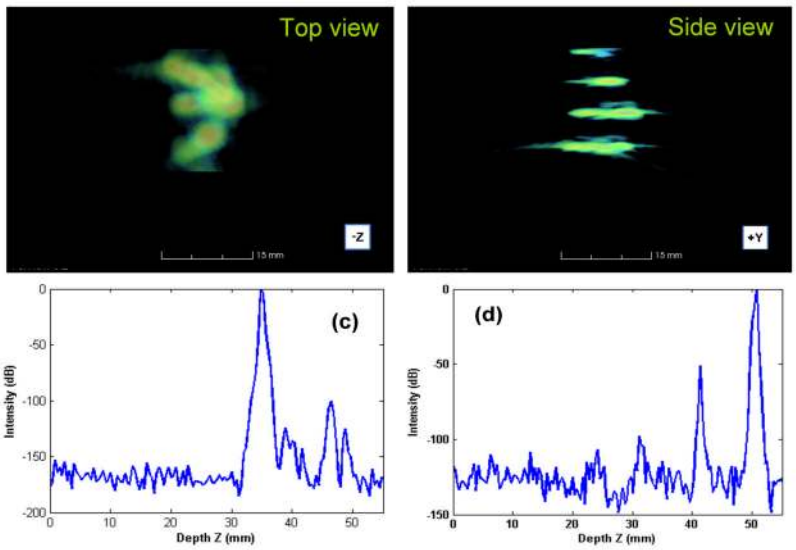

Fig. 5.

(a) Volumetric view, and (b) front view of the photoacoustic images at 70 dB dynamic range. The horse hair strands are at 3.5 cm, 4 cm, 4.5 cm, and 5 cm deep. (c) Line plot for horse hair at 3.5 cm depth and (d) line plot for horse hair at 5 cm depth.

Table 1

Spatial resolution as a function of imaging depth

Object depth (cm)	Axial resolution (μm)	Lateral resolution (μm)
3.5	340	520
4.0	320	500
4.5	520	1100
5.0	680	1200